Electronic Supplement 3

Surface temperature retrieval

In this Supplement we assess the retrieval of surface temperature using two methods:

(1) Deconvolution of the spectral responses for emissivity, transmissivity and atmospheric upwelling radiance, and
(2) Use of bandwidth averaged values.

To do this we consider a nighttime scenario (i.e., there is no reflected radiation) and use MODIS Band 22, which covers the nominal (top-hat response function) wave range of 3.929 μm to 3.989 μm (Barnes et al., 1998). We first set up a sensor model which predicts the sensor recorded brightness temperature through convolution of the expected satellite-arriving radiance with the sensor response function, before deconvolving to obtain surface temperature. We finish by exploring an empirical short-cut that potentially allows us to avoid use of the Planck function when converting between spectral radiance and brightness temperature, or between brightness temperature and spectral radiance.

(A) At-sensor radiance and brightness temperature

At-sensor radiance for a surface radiating at temperature T_s can be assessed through convolution of the spectral radiance from the emitting surface, with spectral emissivity, transmissivity, and upwelling radiance, as well as the sensor response function. The required sequence of convolutions for MODIS Band 22 is given graphically in Figure S3.1. The method to achieve this convolution, thereby allowing an assessment of at-sensor radiance for a given surface temperature is as follows.

1. Input of emisivity, transmissivity, and upwelling radiance spectra

First, the waveband of interest is split into increments of width $d\lambda$. These increments are, here, set to match those given with the sensor response function. By way of example, in Table S3.1 the waveband spectral range and increments are set equal to those given for the spectral response function of MODIS Band 22. In this case, the response function extends

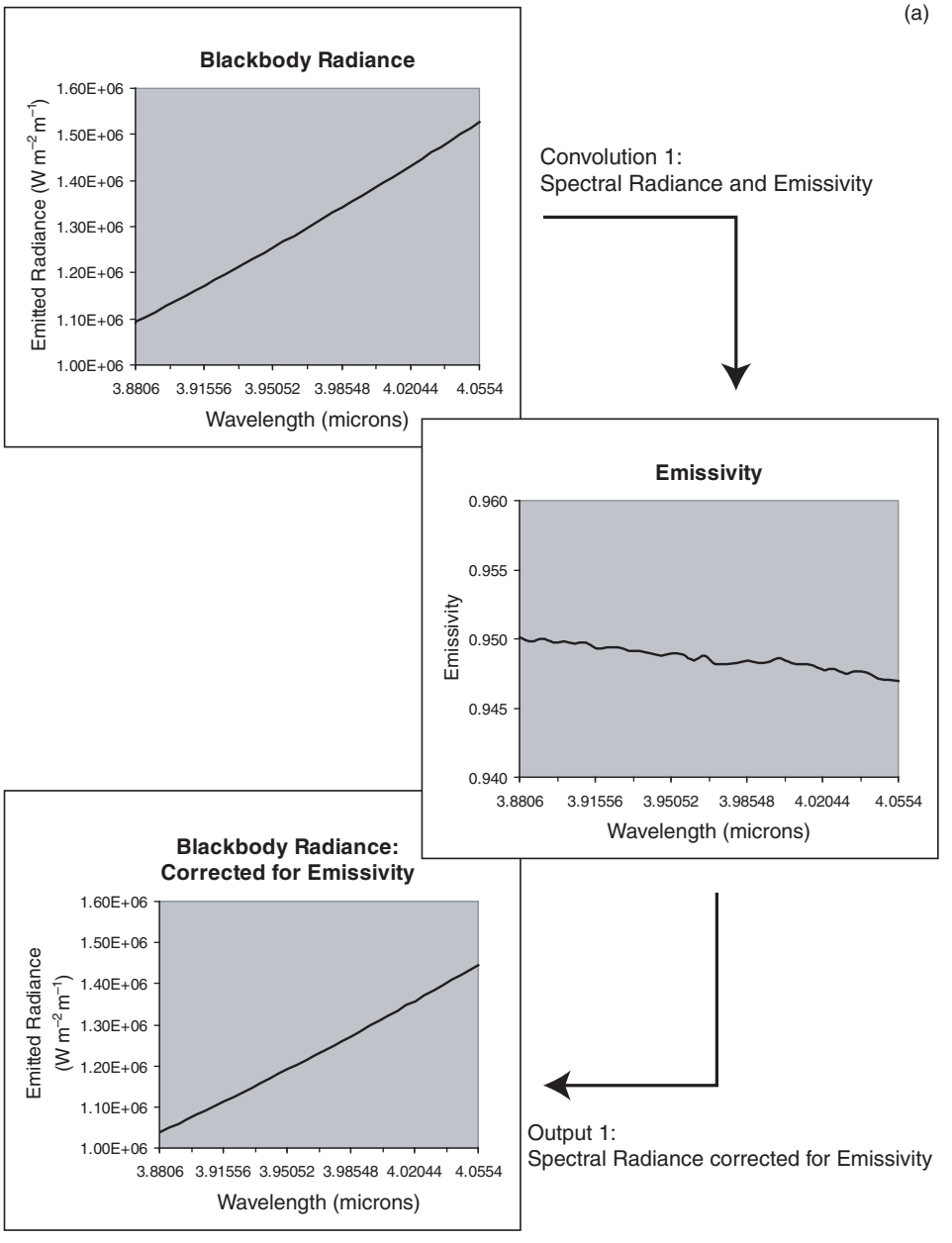

Figure S3.1 Steps to obtain sensor-recorded radiance from surface emitted radiance. (a) Convolution of blackbody spectral radiance (for a surface at 15 °C) with spectral emissivity (for a Hawaiian pahoehoe surface). (b) Convolution of emissivity-corrected spectral radiance with spectral transmissivity (for a surface at sea-level under a US Standard atmosphere). (c) Convolution of emissivity- and transmissivity-corrected spectral radiance with atmospheric up-welling spectral radiance (for a surface at sea-level under a US Standard atmosphere). (d) Convolution of at-satellite spectral radiance with sensor response function to obtain at-sensor spectral radiance.

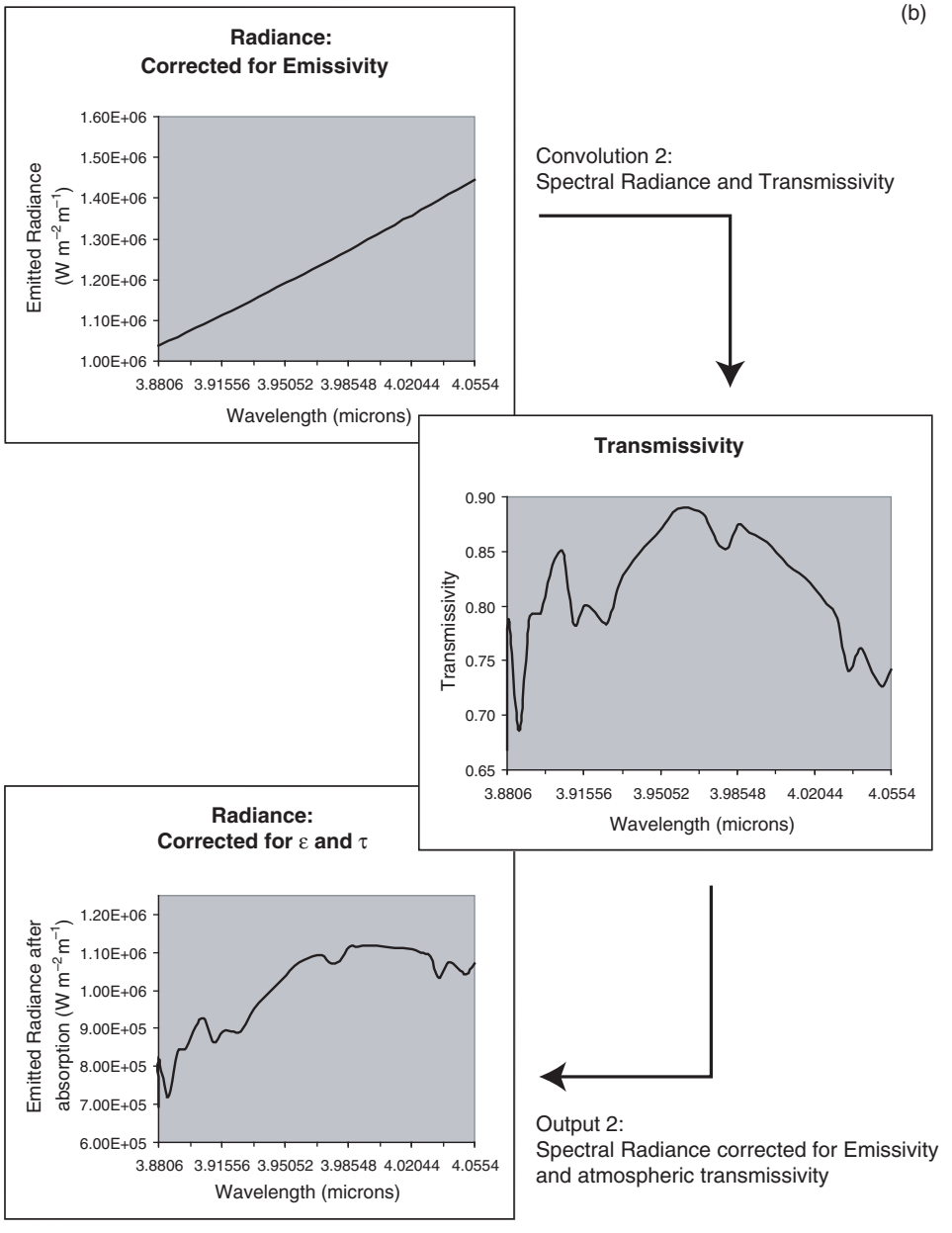

Figure S3.1b (cont.)

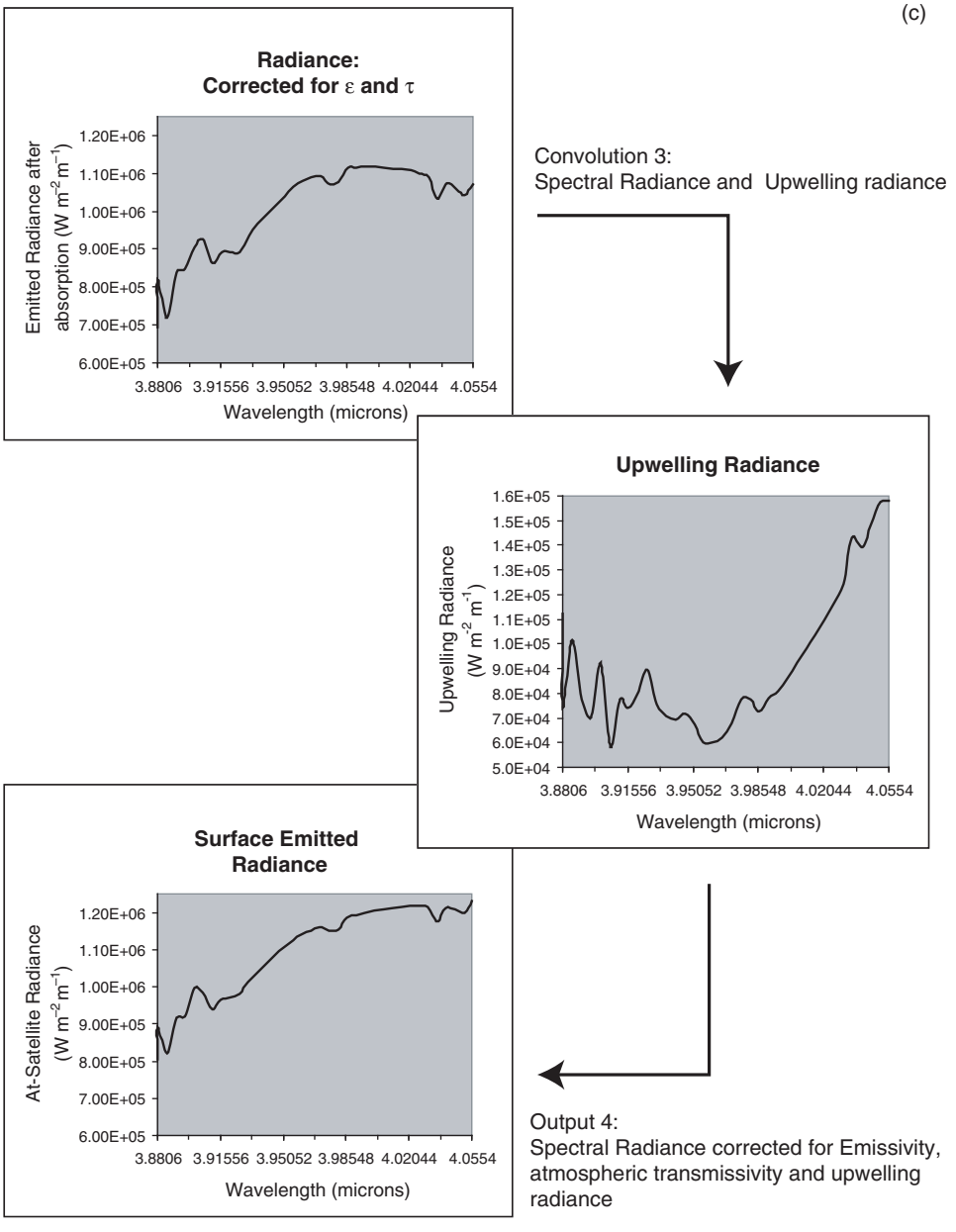

Figure S3.1c (cont.)

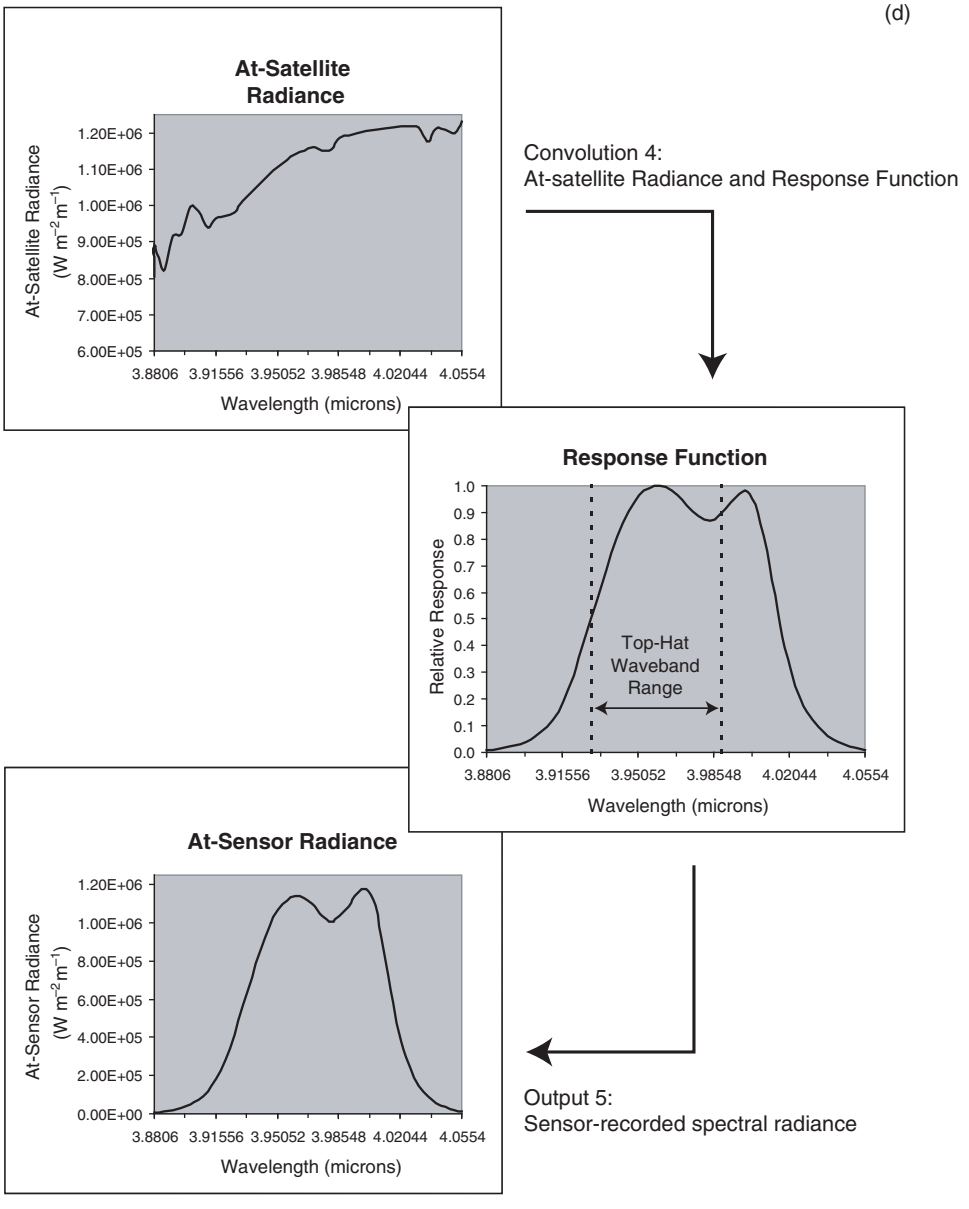

Figure S3.1d (cont.)

between 3.8806 μm and 4.0554 μm, in increments (dλ) of ~0.005 μm. Next, for each dλ increment, spectral emissivity [ε(λ)], transmissivity [τ(λ)] and upwelling radiance [$L_U(\lambda)$] are estimated and input, as shown in Table S3.1.

2. Estimation of at-satellite radiance

Spectral radiance is now calculated for a blackbody radiating at temperature T, with T in this case being set to 15 °C (= 15 °C + 273.15 = 288.15 K). This is achieved using the wavelength appropriate for each dλ increment in the Planck Function, i.e.,

Table S3.1. *Sensor response function for MODIS band 22, with the emissivity, transmissivity and upwelling radiance values for each dλ increment of the response function. The values averaged across the sensor response function wave-range (3.881 μm to 4.055 μm), as well as across the published waveband of MODIS band 22 (3.929 μm to 3.989 μm), are given at the table foot. Emissivity is for Hawaiian pahoehoe collected from Kilauea's Mauna Ulu flow field (Sample: MU1, Table 8.1, Chapter 8). Atmospheric parameters are obtained from MODTRAN using a 1976 US Standard atmosphere (see Electronic Supplement 4).*

Wavelength [λ, μm]	Increment [dλ, μm]	Relative Response [$R_b(\lambda)$]	Emissivity [ε(λ)]	Transmissivity [τ(λ)]	Upwelling Radiance [$L_U(\lambda)$, W m^{-2} m^{-1}]
3.8806	0.0003	0.01	0.9501	0.66891	1.12E+05
3.8809	0.0051	0.01	0.9500	0.78819	7.41E+04
3.8860	0.0050	0.01	0.9498	0.68554	1.01E+05
3.8910	0.0050	0.02	0.9500	0.79116	7.73E+04
3.8960	0.0050	0.03	0.9497	0.79276	7.04E+04
3.9010	0.0049	0.05	0.9499	0.83741	9.27E+04
3.9059	0.0052	0.08	0.9496	0.849	5.84E+04
3.9111	0.0049	0.12	0.9497	0.78286	7.73E+04
3.9160	0.0049	0.19	0.9493	0.80104	7.41E+04
3.9209	0.0051	0.29	0.9494	0.79385	8.01E+04
3.9260	0.0051	0.42	0.9494	0.78457	8.95E+04
3.9311	0.0048	0.56	0.9491	0.81678	7.57E+04
3.9359	0.0051	0.69	0.9491	0.83563	7.07E+04
3.9410	0.0050	0.81	0.9490	0.84831	6.94E+04
3.9460	0.0051	0.90	0.9488	0.85926	7.19E+04
3.9511	0.0048	0.96	0.9489	0.87204	6.72E+04
3.9559	0.0051	0.99	0.9489	0.88597	6.03E+04
3.9610	0.0050	1.00	0.9485	0.88977	6.00E+04
3.9660	0.0049	0.98	0.9488	0.88834	6.22E+04
3.9709	0.0051	0.95	0.9482	0.88286	6.79E+04
3.9760	0.0051	0.90	0.9482	0.85809	7.76E+04
3.9811	0.0049	0.87	0.9483	0.85276	7.73E+04

Table S3.1. (*cont.*)

Wavelength [λ, μm]	Increment [dλ, μm]	Relative Response [$R_b(\lambda)$]	Emissivity [$\varepsilon(\lambda)$]	Transmissivity [$\tau(\lambda)$]	Upwelling Radiance [$L_U(\lambda)$, W m^{-2} m^{-1}]
3.9860	0.0049	0.87	0.9484	0.87464	7.26E+04
3.9909	0.0052	0.91	0.9483	0.8674	7.79E+04
3.9961	0.0050	0.96	0.9484	0.86183	8.11E+04
4.0011	0.0050	0.98	0.9486	0.854	8.61E+04
4.0061	0.0050	0.90	0.9483	0.84347	9.27E+04
4.0111	0.0050	0.70	0.9481	0.83377	9.83E+04
4.0161	0.0048	0.48	0.9481	0.8259	1.04E+05
4.0209	0.0051	0.31	0.9477	0.81581	1.10E+05
4.0260	0.0051	0.20	0.9478	0.80226	1.17E+05
4.0311	0.0048	0.12	0.9475	0.78834	1.24E+05
4.0359	0.0052	0.08	0.9476	0.74011	1.43E+05
4.0411	0.0048	0.05	0.9476	0.76137	1.39E+05
4.0459	0.0052	0.03	0.9472	0.74552	1.48E+05
4.0511	0.0043	0.02	0.9470	0.72649	1.57E+05
4.0554	0.0003	0.01	0.9470	0.74174	1.58E+05
Average (3.881–4.055 μm):		0.47	0.9487	0.8148	9.13E+04
Average (3.929–3.989 μm):		0.88	0.9486	0.8640	7.01E+04

$$R_{BB}(\lambda) = M(\lambda, T) = c_1\lambda^{-5}\left[\exp^{\frac{c_2}{\lambda T}} - 1\right]^{-1} \text{ (W m}^{-2}\text{ m}^{-1}\text{)}$$

in which c_1 and c_2 are 3.741×10^{-16} W m^{-2} and 1.4393×10^{-2} m K. Thus, for the first dλ increment in Table S3.1, λ is 3.8806×10^{-6} m. When completed for each wavelength increment, this gives the blackbody spectral radiance, $R_{BB}(\lambda)$ for a surface emitting at temperature T, as shown in column two of Table S3.2.

$R_{BB}(\lambda)$ at each increment is then corrected as follows:

(1) First, for each spectral increment, $R_{BB}(\lambda)$ is corrected using the emissivity appropriate for that increment to give:

$$R_\varepsilon(\lambda)[= \varepsilon(\lambda)R_{BB}(\lambda)].$$

(2) Second, for each spectral increment, $R_\varepsilon(\lambda)$ is corrected for atmospheric transmissivity to give:

$$R_{\varepsilon,\tau}(\lambda)[= \tau(\lambda)R_\varepsilon(\lambda)].$$

Table S3.2. *Spectral radiance [$R_{BB}(\lambda)$] for a blackbody radiating at 15 °C for each dλ increment defined across the 3.881 μm to 4.055 μm range. $R_{BB}(\lambda)$ is convolved with the emissivity, transmissivity and upwelling radiance spectra given in Table S3.1 to yield $R_{\varepsilon}(\lambda)$, $R_{\varepsilon,\tau}(\lambda)$ and, finally, expected at-satellite radiance [$R^*_{in}(\lambda)$] at each increment. The average radiance obtained at each step, and the brightness temperature that this yields, is given at the foot of the table.*

Wavelength [λ, μm]	$R_{BB}(\lambda)$ [=M(λ,T)] W m^{-2} m^{-1}	$R_{\varepsilon}(\lambda)$ [= $\varepsilon(\lambda)R_{BB}(\lambda)$] W m^{-2} m^{-1}	$R_{\varepsilon,\tau}(\lambda)$ [= $\tau(\lambda)R_{\varepsilon}(\lambda)$] W m^{-2} m^{-1}	$R^*_{in}(\lambda)$ [=$R_{\varepsilon,\tau}(\lambda) + L_U(\lambda)$] W m^{-2} m^{-1}
3.8806	1.09E+06	1.04E+06	6.94E+05	8.06E+05
3.8809	1.09E+06	1.04E+06	8.19E+05	8.93E+05
3.8860	1.10E+06	1.05E+06	7.19E+05	8.21E+05
3.8910	1.12E+06	1.06E+06	8.39E+05	9.16E+05
3.8960	1.13E+06	1.07E+06	8.48E+05	9.19E+05
3.9010	1.14E+06	1.08E+06	9.05E+05	9.98E+05
3.9059	1.15E+06	1.09E+06	9.27E+05	9.85E+05
3.9111	1.16E+06	1.10E+06	8.64E+05	9.41E+05
3.9160	1.17E+06	1.11E+06	8.92E+05	9.66E+05
3.9209	1.18E+06	1.12E+06	8.93E+05	9.73E+05
3.9260	1.20E+06	1.14E+06	8.91E+05	9.81E+05
3.9311	1.21E+06	1.15E+06	9.37E+05	1.01E+06
3.9359	1.22E+06	1.16E+06	9.67E+05	1.04E+06
3.9410	1.23E+06	1.17E+06	9.92E+05	1.06E+06
3.9460	1.24E+06	1.18E+06	1.01E+06	1.09E+06
3.9511	1.26E+06	1.19E+06	1.04E+06	1.11E+06
3.9559	1.27E+06	1.20E+06	1.07E+06	1.13E+06
3.9610	1.28E+06	1.21E+06	1.08E+06	1.14E+06
3.9660	1.29E+06	1.23E+06	1.09E+06	1.15E+06
3.9709	1.30E+06	1.24E+06	1.09E+06	1.16E+06
3.9760	1.32E+06	1.25E+06	1.07E+06	1.15E+06
3.9811	1.33E+06	1.26E+06	1.08E+06	1.15E+06
3.9860	1.34E+06	1.27E+06	1.11E+06	1.19E+06
3.9909	1.36E+06	1.29E+06	1.11E+06	1.19E+06
3.9961	1.37E+06	1.30E+06	1.12E+06	1.20E+06
4.0011	1.38E+06	1.31E+06	1.12E+06	1.21E+06
4.0061	1.39E+06	1.32E+06	1.12E+06	1.21E+06
4.0111	1.41E+06	1.33E+06	1.11E+06	1.21E+06
4.0161	1.42E+06	1.35E+06	1.11E+06	1.22E+06
4.0209	1.43E+06	1.36E+06	1.11E+06	1.22E+06
4.0260	1.45E+06	1.37E+06	1.10E+06	1.22E+06
4.0311	1.46E+06	1.38E+06	1.09E+06	1.21E+06
4.0359	1.47E+06	1.40E+06	1.03E+06	1.18E+06
4.0411	1.49E+06	1.41E+06	1.07E+06	1.21E+06

Table S3.2. (*cont.*)

Wavelength [λ, μm]	$R_{BB}(\lambda)$ [=M(λ,T)] W m^{-2} m^{-1}	$R_{\varepsilon}(\lambda)$ [= ε(λ)$R_{BB}(\lambda)$] W m^{-2} m^{-1}	$R_{\varepsilon,\tau}(\lambda)$ [= τ(λ)$R_{\varepsilon}(\lambda)$] W m^{-2} m^{-1}	$R^*_{in}(\lambda)$ [=$R_{\varepsilon,\tau}(\lambda)$ + $L_U(\lambda)$] W m^{-2} m^{-1}
4.0459	1.50E+06	1.42E+06	1.06E+06	1.21E+06
4.0511	1.51E+06	1.43E+06	1.04E+06	1.20E+06
4.0554	1.53E+06	1.45E+06	1.07E+06	1.23E+06
Average (W m^{-2} m^{-1}):	1.30E+06	1.23E+06	1.00E+06	1.09E+06
Brightness Temperature (°C):	15.0	13.8	9.2	11.1

Note: Emissivity and transmissivity effects result in a decreased brightness temperature (T*), but the addition of the atmospheric upwelling component brings T* back up again.

(3) Finally, the contribution of atmospheric up-welling radiance is added to $R_{\varepsilon,\tau}(\lambda)$ to give the predicted at-satellite radiance at each spectral increment:

$$R^*_{in}(\lambda)\ [= R_{\varepsilon,\tau}(\lambda) + L_U(\lambda)]$$

These steps are executed in sequence across columns three, four and five of Table S3.2.

At-satellite spectral radiance

At-satellite spectral radiance for each increment [$R^*_{in}(\lambda)$, in W m^{-2} m^{-1}] is converted to total radiant exitance emitted by the surface and arriving at the satellite in each increment [$M^*_{in}(\lambda)$, in W m^{-2}] by multiplying by the increment width [dλ in m], i.e.,

$$M^*_{in}(\lambda) = R^*_{in}(\lambda)\ d\lambda\ (\mathrm{W\ m^{-2}})$$

Integration of $M^*_{in}(\lambda)$ across the waveband then gives the total at-satellite radiant exitance for the surface in the given waveband (M_{in}*), i.e.,

$$M_{in}{}^* = \int_{\lambda_{min}}^{\lambda_{max}} R^*_{in}\, d\lambda\ (\mathrm{Wm^{-2}})$$

By dividing by the integral of the spectral increments, this can be used to estimate the effective spectral radiance arriving at the satellite integrated across the waveband (R_{in}*), i.e.,

$$R_{in}{}^* = \frac{M^*_{in}}{\int_{\lambda_{min}}^{\lambda_{max}} d\lambda}\ (\mathrm{W\ m^{-2}\ m^{-1}})$$

These steps are executed, in sequence, in Table S3.3. R_{in}* can now be converted to a brightness temperature, which in the case modeled in Tables S3.1 to S3.3 is 11.4 °C.

Table S3.3. *At-satellite and at-sensor radiances for a surface at 15 °C emitting in the 3.881 μm to 4.055 μm range. Left hand side gives the waveband increments (dλ) defined in Table S3.1, the expected satellite-arriving radiance for each increment [$R^*_{in}(\lambda)$], as calculated in Table S3.2, and the product of $R^*_{in}(\lambda)\, d\lambda$, i.e., satellite-arriving radiant exitance, $M^*_{in}(\lambda)$, at each increment. Right hand side repeats the MODIS band 22 response function, $R_b(\lambda)$, given in Table S3.1. This is convolved with $M^*_{in}(\lambda)$ to give at-sensor radiant exitance at each dλ increment, $M^*_{sens}(\lambda)$. The product of $R_b(\lambda)$ and dλ at each increment is also given. The integration steps necessary to obtain waveband integrated at-satellite and sensor-recorded radiances are given and explained at the Table foot.*

Wavelength [λ, μm]	Increment [dλ, m]	$R^*_{in}(\lambda)$ W m^{-2} m^{-1}	$M^*_{in}(\lambda)$ [= $R^*_{in}(\lambda)$ dλ] W m^{-2}	Response Function $R_b(\lambda)$	$M^*_{sens}(\lambda)$ [= $R^*_{in}(\lambda)R_b(\lambda)d\lambda$] W m^{-2}	$R_b(\lambda)d\lambda$ (m)
3.8806		8.06E+05		0.01		
3.8809	3.00E-10	8.93E+05	2.68E-04	0.01	2.72E-06	3.05E-12
3.8860	5.10E-09	8.21E+05	4.19E-03	0.01	6.01E-05	7.32E-11
3.8910	5.00E-09	9.16E+05	4.58E-03	0.02	9.93E-05	1.08E-10
3.8960	5.00E-09	9.19E+05	4.59E-03	0.03	1.50E-04	1.63E-10
3.9010	5.00E-09	9.98E+05	4.99E-03	0.05	2.46E-04	2.47E-10
3.9059	4.90E-09	9.85E+05	4.83E-03	0.08	3.69E-04	3.75E-10
3.9111	5.20E-09	9.41E+05	4.89E-03	0.12	5.92E-04	6.29E-10
3.9160	4.90E-09	9.66E+05	4.73E-03	0.19	9.00E-04	9.31E-10
3.9209	4.90E-09	9.73E+05	4.77E-03	0.29	1.38E-03	1.42E-09
3.9260	5.10E-09	9.81E+05	5.00E-03	0.42	2.11E-03	2.16E-09
3.9311	5.10E-09	1.01E+06	5.16E-03	0.56	2.89E-03	2.86E-09
3.9359	4.80E-09	1.04E+06	4.98E-03	0.69	3.42E-03	3.29E-09
3.9410	5.10E-09	1.06E+06	5.41E-03	0.81	4.36E-03	4.11E-09
3.9460	5.00E-09	1.09E+06	5.43E-03	0.90	4.91E-03	4.52E-09
3.9511	5.10E-09	1.11E+06	5.64E-03	0.96	5.44E-03	4.91E-09
3.9559	4.80E-09	1.13E+06	5.41E-03	0.99	5.37E-03	4.77E-09
3.9610	5.10E-09	1.14E+06	5.82E-03	1.00	5.82E-03	5.10E-09
3.9660	5.00E-09	1.15E+06	5.76E-03	0.98	5.65E-03	4.91E-09
3.9709	4.90E-09	1.16E+06	5.69E-03	0.95	5.39E-03	4.65E-09
3.9760	5.10E-09	1.15E+06	5.86E-03	0.90	5.29E-03	4.60E-09
3.9811	5.10E-09	1.15E+06	5.88E-03	0.87	5.14E-03	4.46E-09
3.9860	4.90E-09	1.19E+06	5.81E-03	0.87	5.08E-03	4.28E-09
3.9909	4.90E-09	1.19E+06	5.84E-03	0.91	5.33E-03	4.47E-09
3.9961	5.20E-09	1.20E+06	6.24E-03	0.96	5.99E-03	5.00E-09
4.0011	5.00E-09	1.21E+06	6.03E-03	0.98	5.90E-03	4.89E-09
4.0061	5.00E-09	1.21E+06	6.04E-03	0.90	5.44E-03	4.51E-09
4.0111	5.00E-09	1.21E+06	6.06E-03	0.70	4.26E-03	3.52E-09
4.0161	5.00E-09	1.22E+06	6.08E-03	0.48	2.91E-03	2.39E-09
4.0209	4.80E-09	1.22E+06	5.85E-03	0.31	1.83E-03	1.50E-09
4.0260	5.10E-09	1.22E+06	6.21E-03	0.20	1.22E-03	1.01E-09

Table S3.3. (*cont.*)

Wavelength [λ, μm]	Increment [dλ, m]	$R^*_{in}(\lambda)$ W m^{-2} m^{-1}	$M^*_{in}(\lambda)$ [= $R^*_{in}(\lambda)$ dλ] W m^{-2}	Response Function $R_b(\lambda)$	$M^*_{sens}(\lambda)$ [= $R^*_{in}(\lambda)R_b(\lambda)d\lambda$] W m^{-2}	$R_b(\lambda)d\lambda$ (m)
4.0311	5.10E-09	1.21E+06	6.20E-03	0.12	7.61E-04	6.26E-10
4.0359	4.80E-09	1.18E+06	5.65E-03	0.08	4.45E-04	3.78E-10
4.0411	5.20E-09	1.21E+06	6.31E-03	0.05	3.01E-04	2.48E-10
4.0459	4.80E-09	1.21E+06	5.80E-03	0.03	1.66E-04	1.37E-10
4.0511	5.20E-09	1.20E+06	6.24E-03	0.02	9.82E-05	8.19E-11
4.0554	4.30E-09	1.23E+06	5.29E-03	0.01	5.29E-05	4.30E-11
Integral (1):			1.94E-01		9.94E-02	
Integral (2):	1.75E-07					8.74E-08
Integral (1)/(2):			1.11E+06			1.14E-06
T* (°C)			11.4			12.0

Explanation of Table base:

• **Left hand side of the table base:**

Satellite-arriving radiance: We first integrate $M^*_{in}(\lambda)$ (Integral 1) and dλ (Integral 2) across all waveband increments. Dividing Integral (2) by Integral (1) yields the satellite-arriving radiance integrated across the entire waveband (R_{in}*). R_{in}* converts to a brightness temperature (T*) of 11.4 °C.

• **At the right hand side of the table base:**

Sensor-recorded radiance: We first integrate, across all waveband increments, $M^*_{sens}(\lambda)$ (Integral 1) and the product of $R_b(\lambda)d\lambda$ (Integral 2). Dividing Integral (2) by Integral (1) yields the sensor-recorded radiance integrated across the entire waveband (R*). R* converts to a brightness temperature (T*) of 12 °C.

3. Convolution of the sensor spectral response function

R_{in}* is the radiance that would be recorded by a sensor with a perfect spectral response, i.e., the response is 100 % across the waveband and zero outside of it. Given that this is not the case (see Section 3.4 of Chapter 3), the final step is to convolve the spectral response function of the waveband with the effective spectral radiance arriving at the satellite. This yields the effective spectral radiance recorded by the sensor (R*) and is achieved using the spectral responsivity for each wavelength increment, $R_b(\lambda)$, as follows:

$$R^* = \frac{\int_{\lambda_{min}}^{\lambda_{max}} R^*_{in} R_b(\lambda) d\lambda}{\int_{\lambda_{min}}^{\lambda_{max}} R_b(\lambda) d\lambda} \ (\mathrm{W\ m^{-2}\ m^{-1}})$$

The result, for the model followed here, is given on the right hand side of Table S3.3. Table S3.3 shows that the effective spectral radiance recorded by the sensor, in this case, yields a

brightness temperature of 12.0 °C. This is the brightness temperature that will be obtained from the sensor-recorded radiance.

(B) Inversion to estimate surface temperature

Inversion of the sequence described above allows sensor recorded radiance (R*) to be converted back to surface temperature. Deconvolution first involves conversion of the sensor-derived brightness temperature (12 °C) to at-satellite brightness temperature (11.4 °C). The radiance equivalent of the at-satellite brightness temperature is the radiance arriving at the satellite before response function effects [i.e., $R^*_{in}(\lambda)$]. $R^*_{in}(\lambda)$ is then deconvolved with the spectral upwelling radiance, transmissivity and emissivity spectra. That is, for each spectral increment

(1) The contribution of atmospheric up-welling radiance is removed from $R^*_{in}(\lambda)$ to give $R_{\varepsilon,\tau}(\lambda)$,

$$\text{i.e., } R^*_{in}(\lambda) - L_U(\lambda) = R_{\varepsilon,\tau}(\lambda).$$

.

(2) $R_{\varepsilon,\tau}(\lambda)$ is then corrected for atmospheric transmissivity to give $R_\varepsilon(\lambda)$,

$$\text{i.e., } R_{\varepsilon,\tau}(\lambda)/\tau(\lambda) = R_\varepsilon(\lambda).$$

(3) Finally, $R_\varepsilon(\lambda)$ is corrected using the emissivity appropriate for each $d\lambda$ increment to give $R_{BB}(\lambda)$,

$$\text{i.e., } R_\varepsilon(\lambda)/\varepsilon(\lambda) = R_{BB}(\lambda).$$

.

Effectively, we reverse the step sequence given across Tables S3.3 and S3.2 to obtain the blackbody spectral radiance, $R_{BB}(\lambda)$, at each spectral increment for the targeted surface. Total spectral radiance emitted by the surface, and integrated across the waveband (R_{BB}), is now obtained from:

$$R_{BB} = \frac{\int_{\lambda_{min}}^{\lambda_{max}} R_{BB}(\lambda)d\lambda}{\int_{\lambda_{min}}^{\lambda_{max}} d\lambda} \text{ (W m}^{-2}\text{ m}^{-1}\text{)}$$

Inversion of the Planck function now allows surface temperature (T) to be calculated

$$T = \frac{c_2}{\lambda \ln\left(\frac{c_1\lambda^{-5}}{R_{BB}} + 1\right)} \text{ (K)}$$

In this case, we solve using $R_{BB} = 1.30 \times 10^6$ W m^{-2} m^{-1} and the mid-point wavelength of the MODIS Band 22 spectral response function (3.968×10^{-6} m). This yields a temperature of 15 °C, which is equal to the initial surface temperature input into the sensor model (i.e., 15 °C: see foot of Table S3.2).

(C) Use of bandwidth averaged values

A commonly used method converts brightness temperature to surface temperature by simply using band-averaged values. Band-averaged values for the case modeled here are given at the foot of Table S3.1. Using the model developed above for demonstration, this method operates as follows:

(1) First, the sensor-recorded brightness temperature (T* = 12 °C) is converted to a radiance (R*) using the Planck Function with the mid-point of the published waveband range. In this case, the published waveband range is 3.929 to 3.989 μm (Barnes et al., 1998), so $\lambda = 3.959$ μm or 3.969×10^{-6} m. This yields an at-sensor radiance of 1.12×10^6 W m^{-2} m^{-1}.
(2) The at-sensor radiance is corrected for atmospheric and emissivity effects using the band-averaged values for atmospheric upwelling, transmissivity and emissivity in

$$L(\lambda, T_s) = [R^* - L_U(\lambda)]/[\tau(\lambda)\varepsilon(\lambda)]$$

Inputting the values averaged across the 3.929 to 3.989 μm waveband (as given in Table S3.1), this yields:

$$\begin{aligned} L(\lambda, T_s) &= \frac{(1.12x10^6 \mathrm{Wm^{-2}m^{-1}}) - (7.01x10^4 \mathrm{Wm^{-2}m^{-1}})}{(0.8640)(0.9486)} \\ &= 1.28 \times 10^6 \text{ W m}^{-2} \text{ m}^{-1}. \end{aligned}$$

(3) Inverting Planck and inputting this corrected radiance with the waveband mid-point of 3.959 μm now yields a surface temperature of 15.1 °C.

Thus, in this case, surface temperature retrieved using the band-averaged approach, and a brightness temperature uncorrected for response function effects, is within 0.1 °C of the starting value input into the sensor model.

Note:
This band-averaged methodology is valid if both the Planck curve, as well as the emissivity, transmissivity and atmospheric upwelling radiance spectra, are relatively flat across the waveband of interest. This tends to be the case for relatively narrow wavebands in the mid- and thermal-infrared but, as discussed in Chapter 3, may not apply to the following cases:

(1) For broader wavebands,
(2) Wavebands in the NIR and SWIR where the Planck curves for blackbodies at lava temperatures rise steeply, and/or

(2) Wavebands within which emissivity, transmissivity and/or atmospheric upwelling radiance spectra undergo significant variation.

(D) The Singh (1984) short cut

Singh (1984) proposed a short cut for conversion between brightness temperature (T*) and spectral radiance [R*(λ)], whereby

$$Ln[R^*(\lambda)] = a_1 + \frac{b_1}{T^*}$$

so that, the conversion between spectral radiance and brightness temperature is written,

$$T^* = a_1 + \frac{b_1}{Ln[R^*(\lambda)]}$$

This method avoids use of the Planck Function, although the Planck Function does have to be used to initially set the conversion coefficients a_1 and b_1. To apply this empirical approach, Singh (1984) obtained parameters a_1 and b_1 from a least-squares analysis of T* and R*(λ). That is, for the waveband under consideration, temperature versus spectral radiance (as obtained using the Planck Function) was plotted and the best fit between the two obtained. Parameters a_1 and b_1 can only be applied over limited temperature ranges, where Singh (1984) set the relation for AVHRR bands 3 (3.7 μm), 4 (11 μm) and 5 (12 μm) on the TIROS-N, NOAA-6 and -7 satellites by increasing temperature between –3.15 °C and 26.85 °C in increments of 1 °C. For this case, Singh (1984) obtained a correlation coefficient between T* and R*(λ) of better than 0.999 999, and temperatures retrieved by applying the short-cut conversion were within 0.01 °C of the value obtained using the Planck Function.

Such an approach avoids use of the Planck Function in completing the conversions, and hence reduces the number of mathematical operations that need to be applied when completing a temperature-to-radiance, or radiance-to-temperature, conversion. However, as pointed out by Singh and Warren (1983), values of a_1 and b_1 need be set, and must be applied, only over limited temperature ranges, and a relation set for one temperature range will not apply to another.

Applying the short cut

Take the case considered here where we have MODIS band 22 and/or 21 (3.929 μm to 3.989 μm) data with saturation levels of 60 °C and 180 °C, respectively. We apply the approach of Singh (1984) as follows:

(i) We take a temperature range of 0 to 30 °C, and divide the range into 1 °C steps.
(ii) We convert the temperature at each step to a spectral radiance (in W m^{-2} m^{-1}) using the Planck Function (Equation 2.1 of Chapter 2). The function is applied using the central wavelength of the waveband (i.e., 3.959×10^{-6} m for MODIS bands 21 and 22).

(iii) If we plot the derived spectral radiance ($R_{3.959}$*) for each step against brightness temperature (T*, in °C), as done in Figure S3.2a, we can find the best-fit relation. In this case it can be described by,

$$R_{3.959}^{*} = 1774001.9164 \exp^{0.0439(T^{*})},\ R^2 = 0.9992$$

(iv) Plotting brightness temperature (T*) against spectral radiance ($R_{3.959}$*), as done in Figure S3.2b, yields the spectral radiance to temperature conversion, which in this case is,

$$T^{*} = 22.7816\ \mathrm{Ln}(R_{3.959}*) - 327.7870,\quad R^2 = 0.9992$$

(v) If we plot the difference between the temperature used to set the relation and the temperature yielded by the relation, we find that the error from applying the short-cut varies with temperature (Figure S3.2c), yielding an underestimate by 0.5 °C at 0 °C and 30 °C, and an overestimate by 0.5 °C at 15 °C.

The error becomes worse if we apply the relation over ranges extending from 0 °C out to 60 °C or 180 °C (i.e., to the saturation points of bands 21 and 22), where the fit begins to fail badly at higher temperatures (see Figure S3.3). At temperatures of 0°C and 60°C, for example, the error on temperature obtained using the 0 °C to 60 °C exponential relation is 2°C.

For these full range cases, we find that application of a fourth order polynomial provides a better short cut conversion, as given in Figure S3.3. An alternative option is to divide the temperature range into smaller windows, and derive coefficients for each window. This is done in Table S3.4. For this case, we find that if we split the full dynamic range into 10 °C windows, we are able to convert to brightness temperature with an error of less that 0.05 °C. In effect, Table S3.4 can be used as a short cut look-up table to convert between radiance and temperature, or temperature and radiance, with the conversion being applied depending on the radiance, or temperature, being converted. That is, if we have a pixel temperature of 126 °C, we convert to spectral radiance using,

$$R_{3.959}^{*} = 6.48\mathrm{E} + 06 \exp[2.29\mathrm{E} - 02(T^{*})]$$

But if it is 62 °C, we use

$$R_{3.959}^{*} = 2.85\mathrm{E} + 06 \exp\,[3.17\mathrm{E} - 02(T^{*})]$$

We then convert back to brightness temperature using,

$$T^{*} = 43.708\ \mathrm{Ln}\ (R_{3.959}^{*}) - 685.52$$

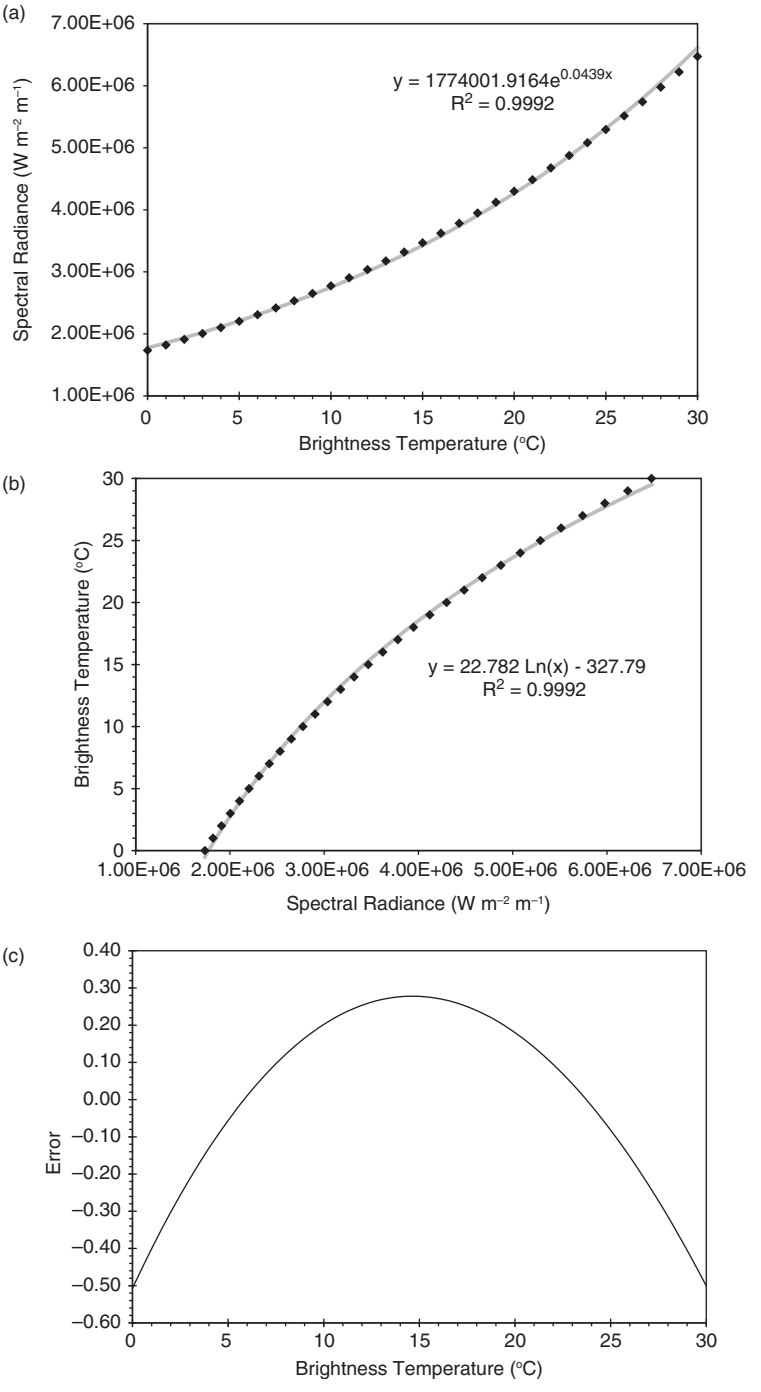

Figure S3.2 Applying the Singh (1984) radiance-temperature-radiance conversion short cut to MODIS bands 21 and 22. (a) Relation between spectral radiance and brightness temperature over the temperature range 0 to 30 °C. (b) Relation between brightness temperature and spectral radiance over the temperature range 0 to 30 °C. (c) Error obtained if the short-cut relation of (b) is used to convert between spectral radiance and brightness temperature.

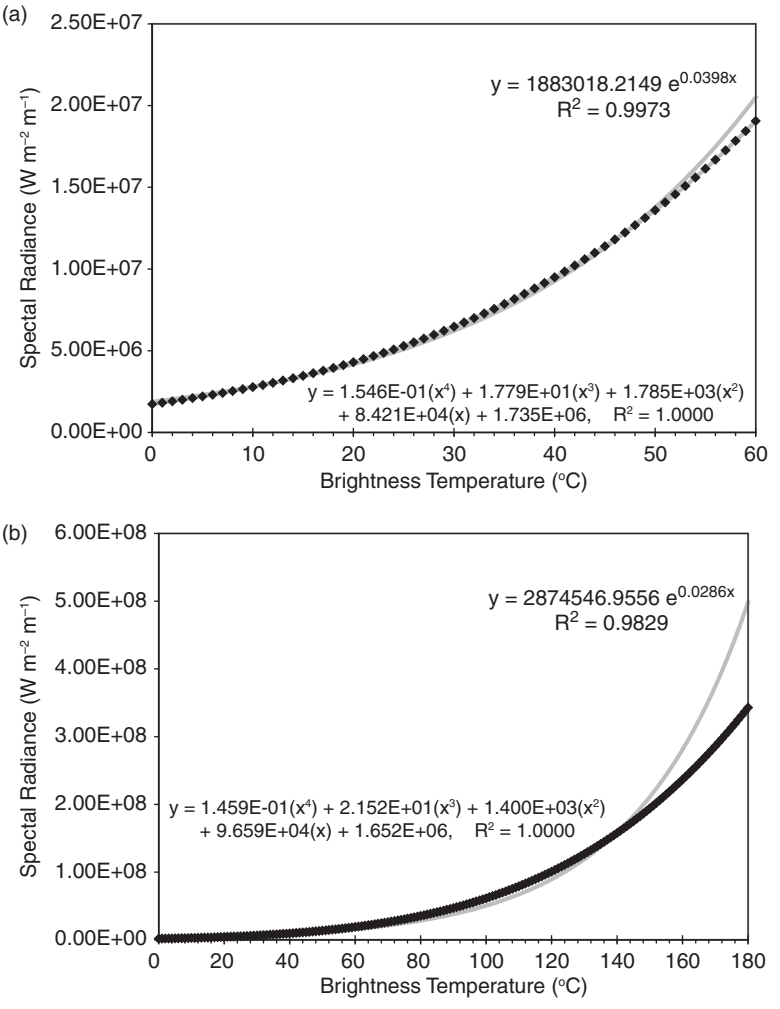

Figure S3.3 Application of the Singh (1984) radiance-temperature-radiance conversion short cut to MODIS bands 21 and 22. (a) Exponential and polynomial relations between spectral radiance and brightness temperature over the temperature range 0 to 60 °C. (b) Exponential and polynomial relations between spectral radiance and brightness temperature over the temperature range 0 to 180 °C. These polynomial relations allow us to convert between temperature and spectral radiance in MODIS bands 21 or 22 over the range 0 to 60 °C, and 0 to 180 °C, respectively. To move between spectral radiance ($R_{3.959}$*) and temperature (T*) we have, for the 0 to 60 °C range,

$$T^* = -1.183E-27(R_{3.959}{}^*)^4 + 6.078E-20(R_{3.959}{}^*)^3 - 1.202E-12(R_{3.959}{}^*)^2 + 1.312E-05\,(R_{3.959}{}^*) - 1.871E+01$$
$$R^2 = 0.9998$$

and for the range 60 to 180 °C,

$$T^* = -2.614E-32(R_{3.959}{}^*)^4 + 2.293E-23(R_{3.959}{}^*)^3 - 7.601E-15(R_{3.959}{}^*)^2 + 1.370E-06(R_{3.959}{}^*) + 3.921E+01$$
$$R^2 = 0.9995$$

We cannot obtain a good full range (0–180°C) fit for the spectral radiance to temperature conversion for this second case.

Table S3.4 *Short cut radiance-temperature-radiance conversions for MODIS bands 21 and 22 derived for each 10 °C window defined between –50 °C and the saturation point of MODIS band 21 (180 °C). The error through applying each short cut conversion is typically <0.05 °C.*

Temperature Range (°C)	Radiance-to-temperature conversion	R^2	Temperature-to-radiance conversion	R^2	Error (°C)
−50 to −41	$T^* = 14.249\ \mathrm{Ln}(R_{3.959}^*) - 212.26$	0.9999	$R_{3.959}^* = 2.95E{+}06\ \exp[7.02E{-}02(T^*)]$	0.9999	≤0.05
−40 to −31	$T^* = 15.529\ \mathrm{Ln}(R_{3.959}^*) - 227.68$	0.9999	$R_{3.959}^* = 2.33E{+}06\ \exp[6.44E{-}02(T^*)]$	0.9999	≤0.05
−30 to −21	$T^* = 16.864\ \mathrm{Ln}(R_{3.959}^*) - 244.62$	0.9999	$R_{3.959}^* = 1.99E{+}06\ \exp[5.93E{-}02(T^*)]$	0.9999	≤0.05
−20 to −11	$T^* = 18.254\ \mathrm{Ln}(R_{3.959}^*) - 263.09$	0.9999	$R_{3.959}^* = 1.82E{+}06\ \exp[5.48E{-}02(T^*)]$	0.9999	≤0.05
−10 to −1	$T^* = 19.699\ \mathrm{Ln}(R_{3.959}^*) - 283.08$	0.9999	$R_{3.959}^* = 1.74E{+}06\ \exp[5.08E{-}02(T^*)]$	0.9999	≤0.05
0 to 10	$T^* = 21.274\ \mathrm{Ln}(R_{3.959}^*) - 305.68$	0.9999	$R_{3.959}^* = 1.74E{+}06\ \exp[4.70E{-}02(T^*)]$	0.9999	≤0.06
11 to 20	$T^* = 22.912\ \mathrm{Ln}(R_{3.959}^*) - 330.00$	0.9999	$R_{3.959}^* = 1.80E{+}06\ \exp[4.36E{-}02(T^*)]$	0.9999	≤0.04
21 to 30	$T^* = 24.528\ \mathrm{Ln}(R_{3.959}^*) - 354.71$	0.9999	$R_{3.959}^* = 1.91E{+}06\ \exp[4.08E{-}02(T^*)]$	0.9999	≤0.03
31 to 40	$T^* = 26.198\ \mathrm{Ln}(R_{3.959}^*) - 380.94$	0.9999	$R_{3.959}^* = 2.07E{+}06\ \exp[3.82E{-}02(T^*)]$	0.9999	≤0.04
41 to 50	$T^* = 27.924\ \mathrm{Ln}(R_{3.959}^*) - 408.69$	0.9999	$R_{3.959}^* = 2.27E{+}06\ \exp[3.58E{-}02(T^*)]$	0.9999	≤0.03
51 to 60	$T^* = 29.704\ \mathrm{Ln}(R_{3.959}^*) - 437.97$	0.9999	$R_{3.959}^* = 2.53E{+}06\ \exp[3.37E{-}02(T^*)]$	0.9999	≤0.04
61 to 70	$T^* = 31.540\ \mathrm{Ln}(R_{3.959}^*) - 468.77$	0.9999	$R_{3.959}^* = 2.85E{+}06\ \exp[3.17E{-}02(T^*)]$	0.9999	≤0.03
71 to 80	$T^* = 33.430\ \mathrm{Ln}(R_{3.959}^*) - 501.09$	0.9999	$R_{3.959}^* = 3.23E{+}06\ \exp[2.99E{-}02(T^*)]$	0.9999	≤0.04
81 to 90	$T^* = 35.376\ \mathrm{Ln}(R_{3.959}^*) - 534.93$	1.0000	$R_{3.959}^* = 3.69E{+}06\ \exp[2.83E{-}02(T^*)]$	1.0000	≤0.03
91 to 100	$T^* = 37.376\ \mathrm{Ln}(R_{3.959}^*) - 570.29$	1.0000	$R_{3.959}^* = 4.23E{+}06\ \exp[2.68E{-}02(T^*)]$	1.0000	≤0.03
101 to 110	$T^* = 39.432\ \mathrm{Ln}(R_{3.959}^*) - 607.18$	1.0000	$R_{3.959}^* = 4.87E{+}06\ \exp[2.54E{-}02(T^*)]$	1.0000	≤0.03
111 to 120	$T^* = 41.542\ \mathrm{Ln}(R_{3.959}^*) - 645.59$	1.0000	$R_{3.959}^* = 5.61E{+}06\ \exp[2.41E{-}02(T^*)]$	1.0000	≤0.04
121 to 130	$T^* = 43.708\ \mathrm{Ln}(R_{3.959}^*) - 685.52$	1.0000	$R_{3.959}^* = 6.48E{+}06\ \exp[2.29E{-}02(T^*)]$	1.0000	≤0.03
131 to 140	$T^* = 46.040\ \mathrm{Ln}(R_{3.959}^*) - 729.06$	1.0000	$R_{3.959}^* = 7.54E{+}06\ \exp[2.17E{-}02(T^*)]$	1.0000	≤0.03
141 to 150	$T^* = 48.435\ \mathrm{Ln}(R_{3.959}^*) - 774.34$	1.0000	$R_{3.959}^* = 8.77E{+}06\ \exp[2.06E{-}02(T^*)]$	1.0000	≤0.02
151 to 160	$T^* = 50.654\ \mathrm{Ln}(R_{3.959}^*) - 774.34$	1.0000	$R_{3.959}^* = 1.01E{+}07\ \exp[1.97E{-}02(T^*)]$	1.0000	≤0.02
161 to 170	$T^* = 52.920\ \mathrm{Ln}(R_{3.959}^*) - 860.48$	1.0000	$R_{3.959}^* = 1.15E{+}07\ \exp[1.89E{-}02(T^*)]$	1.0000	≤0.03
171 to 180	$T^* = 55.361\ \mathrm{Ln}(R_{3.959}^*) - 908.03$	1.0000	$R_{3.959}^* = 1.33E{+}07\ \exp[1.81E{-}02(T^*)]$	1.0000	≤0.03

or

$$T^* = 31.540\ \mathrm{Ln}(R_{3.959}^*) - 468.77$$

This should return brightness temperature to within 0.03 °C of the value that would have been obtained had we used the Planck Function for the conversion.

The method

Thus, to apply the short cut method to another waveband, we need to follow four steps:

(i) Take the waveband dynamic range and split it into windows of 30 °C.
(ii) Across each window, convert temperature to spectral radiance in 1 °C increments.
(iii) Use the result of step (ii) to define the best-fit relation between spectral radiance and temperature, and temperature and radiance, in each window.
(iii) Test the R^2 of the relation and the error on the temperature obtained using the short cut relations, this being the difference between the input temperature used for step (ii) and that derived using the short cut relation.
(iv) If the error is too large, reduce the size of the windows and repeat steps (ii) through (iii).

In the case worked up here in Table S3.4, splitting the –50 °C to 180 °C range into 10 °C windows and deriving a relation for each window results in least squares fits with R^2 of better than 0.9999. The error test of Table S3.4 shows that applying the short cut relations defined for this waveband case will return a brightness temperature that is within 0.05 °C of that returned if the full version of the Planck Function is applied.

References

Barnes, W. L., Pagano, T. S. and Salomonson, V. V. (1998). Prelaunch characteristics of the moderate resolution imaging spectrometer (MODIS) on EOS-AM1. *IEEE Transactions in Geoscience and Remote Sensing*, **36**(4), 1088–1100.

Singh, S. M. (1984). Removal of atmospheric effects on a pixel by pixel basis from the thermal infrared data from instruments on satellites. The Advanced Very High Resolution Radiometer (AVHRR). *International Journal of Remote Sensing*, **5**(1), 161–183.

Singh, S. M. and Warren, D. E. (1983). Sea surface temperatures from infrared measurements. In *Remote Sensing Application in Marine Science and Technology*, ed. A. P. Cracknell, D. Reidel Publishing Company, pp. 231–262.